HHS Public Access

Author manuscript

Oncogene. Author manuscript; available in PMC 2020 January 11.

Published in final edited form as:

Oncogene. 2019 August ; 38(32): 6003–6016. doi:10.1038/s41388-019-0842-2.

Proteomic analysis reveals a role for PAX8 in peritoneal colonization of high grade serous ovarian cancer that can be targeted with micelle encapsulated thiostrepton

Laura R. Hardy, B.A.[1], **Melissa R Pergande, M.S.**[2,*], **Karina Esparza, B.Pharm**[3,*], **Kimberly N. Heath, high school degree**[1], **Hayat Önyüksel, Ph.D.**[3], **Stephanie M. Cologna, Ph.D.**[2], **Joanna E. Burdette, Ph.D.**[1,‡]

[1]Department of Medicinal Chemistry and Pharmacognosy, University of Illinois at Chicago, Chicago, IL, USA.

[2]Department of Chemistry, University of Illinois at Chicago, Chicago, IL, USA.

[3]Department of Biopharmaceutical Sciences, University of Illinois at Chicago, Chicago, IL, USA.

Abstract

High grade serous ovarian cancer (HGSOC) is the fifth leading cause of cancer deaths among women yet effective targeted therapies against this disease are limited. The heterogeneity of HGSOC, including few shared oncogenic drivers and origination from both the fallopian tube epithelium (FTE) and ovarian surface epithelium (OSE), has hampered development of targeted drug therapies. PAX8 is a lineage-specific transcription factor expressed in the FTE that is also ubiquitously expressed in HGSOC where it is an important driver of proliferation, migration, and cell survival. PAX8 is not normally expressed in the OSE, but it is turned on after malignant transformation. In this study, we use proteomic and transcriptomic analysis to examine the role of PAX8 leading to increased migratory capabilities in a human ovarian cancer model, as well as in tumor models derived from the OSE and FTE. We find that PAX8 is a master regulator of migration with unique downstream transcriptional targets that are dependent on the cell's site of origin. Importantly, we show that targeting PAX8, either through CRISPR genomic alteration or through drug treatment with micelle encapsulated thiostrepton, leads to a reduction in tumor burden. These findings suggest PAX8 is a unifying protein driving metastasis in ovarian tumors that could be developed as an effective drug target to treat HGSOC derived from both the OSE and FTE.

‡**Corresponding Author/Off Print Requests:** Joanna Burdette, Associate Professor, University of Illinois at Chicago, Department of Medicinal Chemistry and Pharmacognosy, 833 South Wood Street, 539 PHARM (MC781), Chicago, IL 60612, Tel: 312-996-6153, Fax: 312-996-7101, joannab@uic.edu.

*These authors contributed equally to this work.

Competing Interests: There are no competing interests to declare.

Supplementary information is available at Oncogene's website.

Introduction

High grade serous ovarian cancer (HGSOC) is the most lethal gynecological malignancy[1]. Despite advances in chemotherapy and surgical management, most patients succumb to their disease after developing recurrent tumors and metastasis. The high mortality rate and lack of targeted therapies for ovarian cancer demonstrates the need to identify new drug targets and small molecules that inhibit those targets.

Paired box transcription factor 8 (PAX8) is a lineage-specific transcription factor expressed in the adult fallopian tube epithelium (FTE) and in HGSOC[2]. The ovarian surface epithelium (OSE) does not normally express PAX8, but it is acquired after malignant transformation in multiple mouse models[3,4]. PAX8 overexpression in the OSE induces an epithelial-to-mesenchymal transition with increased migratory capabilities[5,6]. The OSE was originally believed to be the site of ovarian cancer progenitor cells, but recent evidence suggests that the FTE is the main progenitor site[7–9]. Interestingly, knockdown of PAX8 from the healthy FTE had little functional effect and did not significantly alter gene expression[5,10]. PAX8 knockdown in HGSOC, however, decreased cellular proliferation, migration, and invasion while inducing cell death[5,6]. Tumor progression was also attenuated after PAX8 knockdown in ovarian cancer cells[6,11]. Inhibiting PAX8 expression in ovarian cancer therefore has promising therapeutic potential because ovarian tumor cells are reliant on PAX8 while the normal FTE is unaffected by PAX8 reduction. It is important to note that the adult kidney, thyroid, and central nervous system also express PAX8 but mice with PAX8 deleted do not demonstrate defects in the kidney, spinal cord or midbrain/hindbrain boundary[12]. PAX2, which is also expressed in these organs, may be playing a redundant role to rescue the effects of PAX8 deletion. PAX8 plays an essential role in the developing thyroid, but the effect of PAX8 deletion on the adult thyroid remains unknown[12]. Fortunately, there are FDA approved hormone replacement therapies for hypothyroidism that could mitigate any off-target effects of PAX8 targeted therapies against thyroid epithelial cells.

PAX8 acts as both a canonical transcription factor and an epigenetic regulator. In its canonical role, PAX8 has been shown to directly bind and increase transcription of genes driving HGSOC, such as E2F1 and p53[13,14]. The majority of PAX8 binding, however, occurs at non-promoter regions, including enhancer and super-enhancer regions[11]. During malignant transformation to serous carcinoma, PAX8 participates in an interaction with YAP1 that alters its binding sites[10]. The altered PAX8 cistrome may explain the reliance of HGSOC cells on PAX8 despite its minimal role in the normal FTE. In the current work, we use transcriptomic and proteomic approaches to identify pathways regulated by PAX8 in ovarian cancer and in OSE cells. We examine the role of PAX8 on migration in HGSOC as well as in tumor models derived from the OSE and FTE, the two progenitor sites of ovarian cancer. Furthermore, we identify a chemical inhibitor thiostrepton, which upon encapsulation in phospholipid micelles, destabilizes PAX8, reduces tumor growth and metastasis, and increases survival.

Materials and Methods

Cell culture.

OVCAR8^{RFP}, murine ovarian surface epithelium (MOSE), murine oviductal epithelium (MOE), and spontaneously transformed OSE (STOSE) cell lines were cultured as previously described[3,5,15,16]. OVCAR8^{RFP} cells were obtained from Dr. Sharon Stack, University of Notre Dame. STOSE cell lines were obtained from Dr. Barbara Vanderhyden, University of Ottawa[3]. MOE, MOSE-Neo, MOSE-PAX8, and MOE PTEN^{shRNA}KRAS^{G12V} were created previously by our laboratory and cultured as previously described[5,17,18]. Cell lines were demonstrated to be mycoplasma free, STR validated, and pathogen free.

The open-access software CRISPR design (http://crispr.mit.edu/) was used to design guide RNAs (gRNA) targeted to PAX8 exon 3. The forward gRNA (5'-CACCGCATCCGGCCTGGAGTGATAG-3') and reverse gRNA (5'-AAACCTATCACTCCAGGCCGGATGC-3') were annealed and cloned into the pSpCas9 vector (generated by Dr. Feng Zhang, Addgene plasmid #48137), as previously described[19]. OVCAR8^{RFP} and OVCAR4 cells were transfected with 2.5 μg CRISPR plasmid and 2.5 μg pGKpuro plasmid (generated by Dr. Rudolf Jaenisch, Addgene plasmid #11349). Cells were selected using puromycin (0.6 μg/mL) for 48 hours. Single-cell colonies were expanded in media containing puromycin (0.1μg/ml) and validated by Sanger sequencing and immunoblotting (Supplement Figure 1a,b). The Exon 3 F primer (CTA GGG AGA GGG GAT TCC TG) and Exon 3 R primer (AGG AGG CAG GGA GGT ATG AT) were used for sequencing.

Transient transfection of OVCAR8^{RFP} cell lines was performed with either 2.5μg of CMV-PAX8 vector (Transomic, Huntsville, AL, Catalog No. TCM1204) or 2.5μg of PKCαCAT vector (generated by Dr. Bernard Weinstein, Addgene plasmid #21234). Control cells were transfected with pCMV6-XL4-Neo empty vector (OriGene Technologies, Rockville, MD). A PAX8 siRNA (Sigma-Aldrich, St. Louis, MO, EMU061581) was used to knockdown PAX8 in STOSE and MOE PTEN^{shRNA}KRAS^{G12V} cell lines. A luciferase gene siRNA was used as a control (Sigma-Aldrich, St. Louis, MO, EHURLUC). Successful transfections with over-expression vectors and siRNA were verified by immunoblotting (Supplement Figure 1c–f).

RNA-sequencing.

MOSE-neo (2X10^5) and MOSE-PAX8 (1X10^5) cells were plated overnight in a 6-well plate before RNA extraction using Trizol reagent (Life Technologies, Carlsbad, CA) according to the manufacturer's protocol. Residual genomic contamination was removed using RNase-free DNase and RNA was further purified using the RNeasy Mini cleanup (Qiagen, Hilden, Germany). Six RNA libraries (3 technical replicates of MOSE-neo and MOSE-PAX8) were created. Library construction, sequencing, and transcriptome statistical analysis were performed at the Genomics Core Facility at Northwestern University, as previously described[20]. Sequencing data has been deposited in the Gene Expression Omnibus (GEO) database, accession number GSE128751.

Intracellular proteome sample preparation and analysis summary of MOSE-Neo and PAX8 cell lysate samples.

MOSE-neo and MOSE-PAX8 cell pellets (3 biological replicates) were lysed in RIPA buffer and protein concentration was determined using BCA. Each sample was spiked with the internal standard GFP at a concentration of 50fmol per 1µg protein extract and processed via the FASP protocol using triethylammonium bicarbonate buffer[21]. Tryptic peptides were labeled using the 8-plex iTRAQ Reagent kit (AB Sciex, Framingham, MA), according to manufacturer instructions. Peptide mixtures were re-suspended in 0.1% formic acid and purified using SCX (PolyLC, Columbia, MD). The peptide mixture was fractionated followed by mass detection in Auto MS/MS mode with an Agilent 6550 iFunnel Q-TOF LC/MS system coupled to a nano-flow HPLC Chipcube interface[22,23]. Peptides were separated using gradient elution over 70 minutes. Solvent A was 0.1% formic acid where Solvent B was acetonitrile with 0.1% formic acid.

Raw files were converted to .mgf using Proteowizard[24]. MSMS data were searched against the SwissProt Human database, with 2 missed cleavages, MS and MSMS mass error tolerances of 15 ppm and 0.4 Da, respectively. Peptides precursors of +2, +3 and +4 were considered. Variable modifications were: iTRAQ8(Y), oxidation (M) and deamination (NQ), whereas carbamidomethyl (C) and iTRAQ8(K)(N-term) were set as fixed modifications. Protein identifications were accepted at 99.0% probability and contained at least 2 identified peptides using Scaffold Q+. Differentially expressed proteins were determined by applying Permutation Test with unadjusted significance level $p < 0.05$.

SILAC sample preparation and data analysis.

$OVCAR8^{RFP}$ and $OVCAR8^{RFP}PAX8^{-/-}$ clone 2 (3 biological replicates) were plated in T-25 flasks with SILAC DMEM Flex Media (Gibco) and cultured as described previously[25]. Cell pellets were lysed in RIPA buffer and 100ug of heavy and light were mixed at a 1:1 ratio for each biological replicate. Protein digestion was carried out using the FASP method[21] followed by fractionation[23].

Raw data files were searched using Proteome Discoverer against the Human SwissProt database employing a decoy database, using standard settings with global FDR set at 1%. The mass tolerance for precursors was 10ppm and 0.02Da for the fragment ions. Trypsin was set as the protease, allowing two missed cleavages and fixed modification of carbamidomethyl (C) and variable modifications of oxidation (M) and deamidation (NQ). Only proteins with two unique peptides were used for quantitation. Proteomics data can be accessed online at: ftp://massive.ucsd.edu/MSV000083585.

Immunoblot analyses.

Cell lysates for verification of PAX8 alterations in $OVCAR8^{RFP}PAX8^{-/-}$ clones 1 and 2, MOSE-PAX8, STOSE, and MOE $PTEN^{shRNA}KRAS^{G12V}$ cells were collected in RIPA buffer containing protease and phosphatase inhibitors. Protein lysates (20 or 30µg) were electrophoresed on SDS-PAGE gels followed by semi-dry transfer to nitrocellulose membrane. To determine the effect of thiostrepton on the cells, cells were grown in 6-well plates before addition of thiostrepton (10µM) for 24 hours. Combination treatment with

thiostrepton (10μM) and proteasome inhibitor MG132 (10μM) were also performed over 24 hours. Cell lysis and electrophoresis were performed as described above. The antibodies used in these western blots are listed in Supplement Table 1.

Immunofluorescence.

Cells were grown in 8-well chamber slides (Thermo Scientific, Waltham, MA) for 24 hours before fixation and antibody staining, as previously described[26]. Briefly, cells were incubated with a 1:400 dilution of primary mouse anti-vinculin antibody (Sigma, St. Louis, MO) for 1 hour before addition of anti-mouse AlexFlour-488 conjugated secondary antibody. Cells were fixed with rhodamine phalloidin, according to the manufacturer's protocol (Thermo Scientific, Waltham, MA) before mounting using DAPI mounting medium (Vector Laboratories, Burlingame, CA). Images were taken using a Zeiss LSM 710 confocal microscope.

Quantitative RT-PCR.

Cells were grown to 80% confluency before harvest in Trizol reagent (Life Technologies, Carlsbad, CA) and RNA isolation was performed according to the manufacturer's protocol. Total RNA (1μg) was converted to cDNA using the iScript cDNA synthesis kit (BioRad, Hercules, CA). cDNA was amplified using a ViiA7 iCycler real-time SYBR PCR detection system (Life Technologies, Carlsbad, CA). The PAX8 primers were designed to span exon-exon junctions to prevent binding to genomic DNA. Samples were normalized to the housekeeping gene, RNA18S. Three biological replicates were performed.

Cell migration and invasion.

All cell lines tested were grown to 90% confluency before a wound closure assay was performed. A P1000 pipette tip was used to create an artificial wound across a monolayer of cells. Migration of cells across this wound was measured after 24 hours and quantified using ImageJ. Three biological replicates and four technical replicates were performed per migration assay. The inhibitor Go6976 (Sigma, St Louis, MO) was used at 5nM to inhibit PKCα in OVCAR8^{RFP} and OVCAR8^{RFP}PAX8$^{-/-}$ clones 1 and 2[27]. Migration of the STOSE cell line was performed over only 6 hours because of their inherently rapid migratory abilities. Cell migration of the OVCAR8^{RFP} and OVCAR8^{RFP}PAX8$^{-/-}$ clones 1 and 2 was also measured using the xCElligence assay, as previously described[28]. Briefly, 4X10^4 cells were added to the upper chamber of the xCelligence plate (ACEA Bioscience, San Diego, CA) in minimal OVCAR8 media lacking FBS. Media containing 10% FBS was added to the lower chamber of the plate as a chemoattractant. Cell migration towards the lower chamber was measured through changes in electrical impedance every 15 minutes for 48 hours. A matrigel invasion assay was performed for OVCAR8^{RFP}, OVCAR8^{RFP}PAX8$^{-/-}$ clones 1 and 2, MOSE-Neo, and MOSE-PAX8 cells, as previously described[18]. Briefly, 1X10^5 cells were added to a 0.8μM hanging insert (EMD Millipore Sigma, Burlington, MA) coated with 35μg of matrigel (Fisher, Hampton, NH). After 24 hours, cells that did not invade through the matrigel were washed away with PBS while invaded cells were stained with crystal violet (Sigma, St. Louis, MO) and quantified using ImageJ. Images were obtained using an AmScope MU900 with Toupview software (AmScope, Irvine, CA).

Encapsulation of thiostrepton in sterically stabilized micelles (SSM).

Materials—1,2-Distearoyl-sn-glycero-3-phosphoethanolamine-N-methoxy-poly (ethylene glycol 2000) sodium salt (DSPE-PEG_{2000}) was purchased from LIPOID GmbH (Ludwigshafen, Germany). Thiostrepton was obtained from Millipore Sigma (Burlington, MA). Phosphate-buffered saline (PBS) 10X pH 7.4 was purchased from Corning Inc. (Corning, NY) and tert-butanol from Sigma Aldrich (Saint Louis, MO).

Preparation of thiostrepton-SSM nanomedicine.—Preparation of thiostrepton in micelle was performed as previously described[29]. Briefly, thiostrepton was dissolved in tert-butanol and stirred for at least 30 minutes with a magnetic stir bar. In a separate container, DSPE-PEG_{2000} was dissolved in 2X PBS pH 7.4 using sonication. DSPE-PEG_{2000} solution was slowly added onto thiostrepton solution under constant stirring to obtain a 50% tert-butanol: PBS co-solvent system containing 278 μM of thiostrepton and 5mM of DSPE-PEG_{2000}. This formulation was placed in the −80°C freezer overnight and freeze-dried for 24h using a Labconco Freeze Dry System Freezone 4.5 (Kansas City, MO). Lyophilized samples were reconstituted in deionized water with gentle swirling before use.

Characterization of thiostrepton-SSM nanomedicine.—The particle size of thiostrepton-SSM was analyzed by dynamic light scattering using NICOMP® 380 ZLS (Santa Barbara, CA). The drug content was confirmed by high-performance liquid chromatography (HPLC) using a Shimadzu Prominence HPLC system (Kyoto, Japan). Experiments were conducted at room temperature using an Agilent SB-C18 column (250 × 4,6 mm, 5 μm), gradient elution from 30% to 100% of acetonitrile in water with 0.1% trifluoroacetic acid, the flow rate was 1 mL/min, injection volume of 10 μL, and ultraviolet detection was performed at 254nm.

In vivo studies.

Experimental Animals—Six week old female athymic nude mice were purchased from Taconic Farms (Husdon, NY) and delivered to the UIC Animal Care Facility, housed in isolated conditions, and allowed to adapt to their new environment for 2 weeks. Five animals were used per experimental group to obtain 80% power to detect an effect size of 1.6, where effect size is defined as the mean difference between conditions divided by the within condition standard deviation. This assumes a two-tailed test and a Type I error rate of 5%. Blinding was not performed for these studies. All studies were approved by the UIC Animal Care Committee.

Cell collection—All cells (OVCAR8^{RFP} and OVCAR8^{RFP}PAX8$^{-/-}$ clones) were collected using trypsin-EDTA, neutralized with FBS containing media, washed and re-suspended in PBS. Each mouse received 5X10^6 cells in 300uL PBS by intraperitoneal (i.p.) injection.

Survival Study—For the survival study, athymic nude mice (5 mice/group) were inoculated i.p. with OVCAR8^{RFP} or OVCAR8^{RFP}PAX8$^{-/-}$ clones (5X10^6 cells in 300uL PBS). Tumor growth was monitored weekly using the Perkin Elmer (Waltham, MA) IVIS Spectrum *In Vivo* Imaging System (excitation wavelength = 570nm, emission wavelength =

620nm, exposure = 2sec). Mice were sacrificed at humane endpoints and necropsy was performed.

Therapeutic Study—Two groups of female athymic nude mice (5 mice/group) were inoculated i.p. with OVCAR8^{RFP}cells (5X10^6 cells in 300uL PBS). Tumors were allowed to establish for 1 week and mice were equally distributed to treatment groups based on IVIS tumor burden. Tumor growth was monitored using IVIS imaging. The control group received i.p. injection of sterically stable micelle (SSM) alone. The treatment group received i.p. injection of thiostrepton encapsulated sterically stable micelle (TST-SSM) three times weekly. During week one, each mouse received 5mg/kg/dose. Subsequently, each mouse received 20mg/kg/dose. After 4 weeks of injections, the mice were sacrificed, and tumors were collected for IHC and immunoblotting.

Statistics.

All analyses were performed using the Graphpad Prism software (La Jolla, CA). Variance across means was determined prior to statistical analysis. Comparisons of the mean between two samples were analyzed using the paired t-test. Comparisons of the mean for more than two samples were analyzed using either the One-way ANOVA or Two-way ANOVA test. Multiple comparisons to a single control mean were analyzed using the Dunnett's test while multiple comparisons across all means were analyzed using the Tukey's test. The Sidak multiple comparison test was performed following analysis with a Two-way ANOVA. A Kaplan-Meier curve was generated for survival data and it was analyzed using the Logrank test.

Results

Global proteomic analysis of PAX8 regulated pathways.

PAX8 reduction was previously shown to trigger apoptosis in ovarian cancer cells as well as increase expression of pro-migratory genes. We used CRISPR genomic editing to delete PAX8 from the HGSOC cell lines OVCAR8^{RFP} and OVCAR4. Successful deletion of PAX8 in two OVCAR8^{RFP} clones (clones 1 and 2) was confirmed by Sanger sequencing and immunoblotting and these clones were subsequently selected for further study (Supplement Figure 1a, b). Our previous work showed that PAX8 upregulates FOXM1 levels in HGSOC cell lines[5]. We therefore confirmed that PAX8 deletion reduces FOXM1 in the OVCAR8^{RFP} cells (Supplement Figure 1b). Attempts to create a homozygous PAX8 deletion in OVCAR4 were unsuccessful, suggesting this genomic deletion is lethal. Instead, we created an OVCAR4 clone with heterozygous PAX8 deletion that had a decrease in FOXM1 (Supplement Figure 2). Previously published work examined the transcriptome of ovarian cancer cells with PAX8 alteration[10,30]. While RNA-sequencing and transcriptomic analysis provides information about the role of PAX8 as a transcription factor, this method does not elucidate the phenotypic and functional effects of PAX8 in HGSOC. Therefore, we performed mass spectrometry-based differential proteomic analysis on the HGSOC cell line OVCAR8^{RFP} and normal murine OSE (MOSE) cell lines after PAX8 alteration (Supplement Table 2 and 3).

Gene ontology analysis was performed to compare the role of PAX8 when it was deleted from OVCAR8^{RFP} or in MOSE cell lines with PAX8 overexpressed. This analysis showed enrichment of pathways involved in cytoskeletal alterations and cadherin binding in cells expressing PAX8 (Fig. 1a, c). While there were a similar number of proteins significantly altered by PAX8 in OVCAR8^{RFP} (482 proteins) and MOSE (534 proteins), only 28 proteins were differentially altered in both cell lines compared to control (Supplement Table 4). We have previously shown that PAX8 increases expression of N-Cadherin (CDH2) in MOSE, and the proteomics datasets in this study confirms that CDH2, a key mediator of cell adhesion, is upregulated by PAX8 in both MOSE and OVCAR8 (Fig. 1b, d). By immunoblotting, we confirm that PAX8 regulates CDH2 in both OVCAR8 and OVCAR4 cells (Supplement Figure 1,2). Protein kinase Cα (PKCα), on the other hand, is one of the top upregulated proteins by PAX8 in OVCAR8, but it is not significantly altered in MOSE (Fig. 1b). Alternatively, the actinin filaments ACTN1 and ACTN4 are increased by PAX8 in the MOSE cell line, but not in OVCAR8 (Fig. 1d).

PAX8 increases adherens junctions in the OSE.

As an orthogonal approach to examine genes and pathways regulated by PAX8, we performed RNA-sequencing of MOSE-PAX8 cells (Supplement Table 5). PAX8 altered 4,257 transcripts in MOSE-PAX8 cells, suggesting its acquisition can significantly impact the transcriptional landscape of the OSE. Globally, 187 of the 567 proteins significantly regulated by PAX8 in the proteome were found to also be regulated by PAX8 in the transcriptome. Gene set enrichment analysis (GSEA) of the transcriptome and proteome for MOSE-PAX8 cells identified the KEGG adherens junction pathway as differentially regulated in both datasets (Fig. 2a). We have previously shown that PAX8 overexpression in the OSE increases migration and EMT. Here, we further characterize the migratory phenotype by demonstrating increased invasion in MOSE-PAX8 cells (Fig. 2b). Since the GSEA identified ACTN1 and ACTN4 as drivers of adherens junction in MOSE-PAX8 cells, we performed confocal microscopy to examine the localization of actin within the cell. Using immunofluorescence, we show that colocalization of actin and vinculin at the cell surface, a marker of cell adhesion, is markedly increased in MOSE-PAX8 cells (Fig. 2c), suggesting a mechanism for the migratory phenotype observed in these cells.

PAX8 increases migration in HGSOC tumor cells.

Based on our previous data and on the identification that PAX8 regulates the cytoskeleton, we hypothesized that PAX8 may regulate migration and metastasis in ovarian cancer cells. To test this hypothesis, we performed several *in vitro* assays of migration comparing OVCAR8^{RFP} and OVCAR8^{RFP}PAX8$^{-/-}$ clones. PAX8 deletion decreased migration in a wound closure and xCELLigence assay (Fig. 3a, b). Overexpression of PAX8 in the OVCAR8^{RFP}PAX8$^{-/-}$ clones by transfection with a CMV-PAX8 vector rescued their migratory defect (Fig. 3a). Notably, OVCAR8^{RFP}PAX8$^{-/-}$ clone 1 with CMV-PAX8 transfection had increased migration rates compared to the wild type OVCAR8^{RFP} cells. A Boyden chamber assay of invasion demonstrated PAX8 deletion also decreased the invasive ability of ovarian cancer cells (Fig. 3c). The migration and invasion assays described were performed for 24 hours. To control for the effect of cellular proliferation on the migration and invasion assays, an SRB assay was performed over 24 hours for OVCAR8^{RFP} and

OVCAR8^{RFP}PAX8$^{-/-}$ clones. PAX8 deletion did not affect proliferation rate at this time point (Supplement Figure 3). To examine if PAX8 increases adherens junctions in the OVCAR8^{RFP} cell line in a similar manner to the OSE, immunofluorescence was performed for co-localization of actin and vinculin. PAX8 deletion did not alter the cytoskeleton in the OVCAR8^{RFP} cells (Supplement Figure 4). These results functionally confirm our proteomics findings that PAX8 increases migration in the HGSOC cell line OVCAR8, but the mechanism of this increased migration is different than in the OSE, where PAX8 upregulation increased adherens junctions.

To address the effect of PAX8 on tumor cells derived from the OSE or FTE, we knocked down PAX8 in spontaneously transformed OSE (STOSE) and in MOE PTEN^{shRNA}/KRAS^{G12V} tumor cells. These tumor models of ovarian cancer are derived from the murine ovary and oviduct, respectively. PAX8 knockdown reduced migration in both STOSE and MOE PTEN^{shRNA}/KRAS^{G12V} ($p<0.05$) (Fig. 3d, e), demonstrating that PAX8 increases migration in ovarian cancer regardless of the tumor's cell of origin.

Activation of PKCα by PAX8 increases migration in HGSOC.

Our proteomic analysis identified PKCα as a top differentially expressed protein after PAX8 deletion in OVCAR8^{RFP}. We confirmed by immunoblotting that OVCAR8^{RFP} cells express higher levels of PKCα than OVCAR8^{RFP}PAX8$^{-/-}$ clones (Fig. 4a). In MOSE cells, however, PAX8 overexpression did not affect PKCα levels (Supplement Figure 5). To investigate the functional significance of increased PKCα, we performed a wound closure assay for migration using the PKCα inhibitor Go6976. Inhibition of PKCα reduced migration in OVCAR8^{RFP} but this inhibition had no effect on migration on the OVCAR8^{RFP}PAX8$^{-/-}$ clones with already reduced PKCα levels (Fig. 4b). Conversely, transfection with a vector containing the PKCα catalytic domain (PKCαCAT) increased migration in OVCAR8^{RFP}PAX8$^{-/-}$ cells but not in OVCAR8^{RFP} cells (Fig. 4c). These findings suggest the increased migratory potential of OVCAR8^{RFP} compared to OVCAR8^{RFP}PAX8$^{-/-}$ is due to upregulation of PKCα by PAX8.

PAX8 loss attenuates HGSOC progression.

We next examined if the migratory defect in OVCAR8^{RFP}PAX8$^{-/-}$ cells affected *in vivo* tumorigenicity. Mice injected i.p. with OVCAR8^{RFP}PAX8$^{-/-}$ developed tumors later than mice injected with OVCAR8^{RFP} (Fig. 5a, b) and survived longer ($p=0.03$ by log-rank test; Fig. 5c). Mice injected with OVCAR8^{RFP} had a mean survival of 66 days as compared to a mean survival of 77 days for mice injected with OVCAR8^{RFP}PAX8$^{-/-}$ clone 1. Over half the mice injected with OVCAR8^{RFP}PAX8$^{-/-}$ clone 2 survived until the end of the study (day 88). Histological analysis confirmed clones 1 and 2 had no detectable PAX8 protein within the tumor cells (Fig. 5d). Proliferation rate, which was quantified as the number of positive Ki67 cells, demonstrated that tumors containing PAX8 proliferated faster than tumors with PAX8 deleted (114 cells for OVCAR8^{RFP} versus 63 cells and 54 cells for clones 1 and 2, $p<0.01$; Fig. 5d). PAX8 deletion also reduced PKCα levels *in vivo*, validating our previous *in vitro* findings (Fig. 5e). These data indicate that PAX8 is an important component of HGSOC tumors that drives tumor progression and aggressiveness.

Thiostrepton is a chemical inhibitor of PAX8 protein stability.

Thiostrepton is a thiopeptide antibiotic that has been studied in the oncology field for its ability to reduce FOXM1[31]. We show that in the murine oviductal epithelial (MOE) and OVCAR8 cell line, both of which normally express PAX8, exposure to thiostrepton reduces PAX8 protein levels (Fig. 6a). Reduction in FOXM1 is not responsible for this decrease, since FOXM1 knockdown did not affect PAX8 levels (Fig. 6b). Though it has previously been shown that thiostrepton reduces transcription of FOXM1[31–33], thiostrepton actually increases PAX8 transcription (Fig. 6c). Thiostrepton is also able to reduce PAX8 protein in MOSE-PAX8 cells, which are stably transfected with a constitutive CMV-PAX8 (Fig. 6d). These findings taken together suggest thiostrepton does not affect PAX8 transcription. Micrococcin, like thiostrepton, is a thiopeptide antibiotic with similar structure and mechanism of action for inhibition of ribosomal translation in prokaryotes. PAX8 levels were unchanged after exposure to micrococcin, suggesting a unique mechanism of action for thiostrepton (Supplement Figure 6). To determine if thiostrepton upregulates proteasome activity to degrade PAX8, we combined thiostrepton with the proteasome inhibitor MG132. Stabilization of the p53 protein demonstrates that MG132 is an effective proteasome inhibitor, but MG132 was unable to rescue protein degradation induced by thiostrepton (Fig. 6e), suggesting that thiostrepton induces PAX8 degradation in a proteasome independent manner.

Targeting PAX8 using thiostrepton-SSM nanomedicine reduces tumor growth.

Our initial attempts to use un-encapsulated thiostrepton (250mg/kg) dissolved in 30% DMSO to reduce OVCAR8^{RFP} tumor burden were unsuccessful due to toxicity and solubility issues. Mice treated with free thiostrepton began to lose weight after one week of treatment and had to be sacrificed within three weeks of treatment due to toxicity. Upon sacrifice, precipitated thiostrepton had deposited on the peritoneal organs of mice in the treatment group. We therefore encapsulated thiostrepton in sterically stabilized micelles (SSM), which are safe and effective water-soluble nanocarriers composed of PEGylated phospholipid, DSPE-PEG$_{2000}$ (Fig. 7a). When placed in aqueous media above the critical micellar concentration (1 μM), DSPE-PEG$_{2000}$ molecules self-assemble into a core-shell structure with hydrophobic acyl chains forming the core and hydrophilic PEG facing the surface[34]. The hydrophobic core is capable of accommodating water-insoluble drugs, while the hydrated PEG layer confers protection against biological elimination[35]. Thiostrepton-SSM (TST-SSM) and empty micelles (SSM) used as a control exhibited a particle size of approximately 13 nm (intensity-weighted) (Fig. 7a). The drug concentration of TST-SSM samples was within 10% of the calculated concentration. Mice injected i.p. with TST-SSM had significantly reduced tumor burden compared to mice injected i.p. with SSM alone (Fig. 7b). Quantification of total radiant efficiency indicates the therapy reduced tumor burden after 3 weeks of treatment (Fig. 7c). Immunoblotting of tumor tissue protein demonstrated that the TST-SSM treatment was capable of reducing FOXM1 and PAX8 levels *in vivo* (Fig. 7d). Immunohistochemistry verified our earlier result that PAX8 reduction leads to decreased PKCα levels, after both genomic deletion of PAX8 (Fig. 5e) and treatment with TST-SSM (Fig 7e).

Discussion

HGSOC is a heterogeneous disease with few shared genetic alterations between patients. PAX8 is expressed in 99% of serous tumors and affects tumor cell proliferation, morphology, and survival[5,6,36,37]. Several RNA-sequencing studies have been performed to identify the transcriptional targets of PAX8 that lead to these pro-tumorigenic effects[10,11,30]. In this study, we present the first mass spectrometry based proteomic analysis of cell lines after PAX8 alteration to obtain a more phenotypic picture of pathways regulated by PAX8. Proteomic analyses identified PAX8 as a driver of migration and invasion in both the OSE and HGSOC and we validated these findings with functional assays. Our study also identified a small molecule capable of reducing PAX8 protein levels and reducing tumor burden in an ovarian cancer model.

Our previous work examined the role of PAX8 in cells derived from the OSE and FTE, the two progenitor sites of HGSOC. PAX8 is normally expressed in the adult FTE, but we showed that PAX8 deletion from the FTE did not have an obvious phenotypic effect[5]. This finding was validated by RNA-sequencing that demonstrated PAX8 deletion from the FTE did not significantly alter gene expression[10]. Conversely, the OSE does not normally express PAX8, but forced expression of PAX8 increased the malignant potential of these cells. PAX8 expression has also been reported in transgenic mouse models derived from the OSE[3,4]. We therefore performed our proteomic analysis on MOSE-PAX8 cells and compared the protein alterations to OVCAR8^{RFP}PAX8$^{-/-}$ cells. Both isobaric labeling strategies used in this study (SILAC and iTRAQ) have been used to identify differential proteins in a number of biological studies[38–41]. The most notable difference between these methods is the ability to multiplex within an experiment. In both the OSE and HGSOC, PAX8 regulated cytoskeletal structure, but only 28 proteins were regulated by PAX8 in both cell lines. Elias et al. demonstrated that alterations to the PAX8 transcriptional binding motif, or to PAX8 binding partners, are responsible for differences in the cistrome across FTE and HGSOC cell lines[10]. We hypothesize that these alterations to the cistrome are responsible for the unique proteins regulated by PAX8 in our MOSE and OVCAR8 cell line.

Since our analyses identified PAX8 regulated cytoskeleton structure in both the MOSE and OVCAR8 cell lines, we characterized the migratory and invasive capabilities of serous tumor cells derived from the OSE, FTE, and human HGSOC. In tumors derived from the OSE and FTE, PAX8 played a unifying role driving the migratory capability of serous tumors. The downstream effectors regulated by PAX8, however, were unique to each cell type. PKCα was one of the top differentially regulated proteins in the OVCAR8 proteomic dataset but not in the MOSE dataset. In contrast, PAX8 regulated ACTN1 and ACTN4 levels in the MOSE cell line to increase adherens junctions but not in OVCAR8. These findings demonstrate the essential role of PAX8 as an upstream regulator of migration despite unique modes of action across cell types. Previous work characterizing the DNA binding sites of PAX8 using ChIP-sequencing showed lineage and tumor specificity for PAX8 regulated genes[10]. ACTN1, for example, was identified as containing a PAX8 binding site in one cell line out of six, while ACTN4 binding was identified in two cell lines. There were no PAX8 binding sites identified near the PKCα gene in the cell lines tested, but PAX8 was shown to bind near PKCβ, PKCγ and PKCε. We hypothesize that in OVCAR8, PAX8 may acquire a

DNA binding site near PKCα. Alternatively, PAX8 has been shown to be a master regulator of transcription that binds at superenhancer regions[11]. These PAX8 binding sites change during malignant transformation to serous carcinoma. Further experiments will be needed to determine if PAX8 regulates PKCα directly or through binding at superenhancer regions. Here, we show that PAX8 binding is both lineage and tumor specific, yet its regulation of migration is conserved across the cell types examined. PAX8 deletion using CRISPR genomic editing attenuated tumor progression and prolonged survival. Together, these findings suggest PAX8 is a valuable drug target that could reduce the metastasis and increase the survival of HGSOC patients, regardless of cell of origin.

Thiostrepton is a thiopeptide antibiotic that specifically binds the 70S prokaryotic ribosome to inhibit translation[42]. The eukaryotic translational machinery is unaffected by thiostrepton[42]. Thiostrepton has been shown to inhibit transcription of FOXM1[31]. FOXM1 is an oncogene activated in over 80% of HGSOC tumor samples and it is a key driver of serous tumor progression[43]. In this study, we show that thiostrepton decreases PAX8 protein levels in a proteasome independent manner and therefore could be used therapeutically to inhibit both PAX8 and FOXM1, two important regulators of HGSOC aggressiveness. Previous studies have performed *in vivo* thiostrepton treatments at a large range from 30mg/kg to 500mg/kg[33,44]. Our initial attempts at direct i.p. administration of thiostrepton (250mg/kg/week) to reduce serous tumor burden failed because of solubility and toxicity issues. However, the encapsulation of lower doses of thiostrepton in DSPE-PEG_{2000} micelles improved the drug's aqueous solubility and allowed safe administration to animals. By encapsulating thiostrepton in micelles, we were able to supply thiostrepton in a molecular form that is available to interact with the target rather than forming drug aggregates, which are inactive and require longer time to release individual active molecules. Through this delivery method, we achieved therapeutic response to thiostrepton at a lower dose than previously achieved. The encapsulated thiostrepton treatment reduced PAX8 *in vivo* and inhibited tumor progression, highlighting the therapeutic potential of targeting PAX8 in HGSOC. Future work should examine the regulators of PAX8 protein stability that may be affected by thiostrepton, such as PAX8 SUMOylation, which has been shown to increase PAX8 protein stability in thyroid cells[45].

The global proteomic and transcriptomic analyses of PAX8 regulated pathways described here demonstrates the unifying role of PAX8 as a driver of migration and peritoneal colonization in serous tumors derived from the OSE, FTE, and human HGSOC cell lines. Targeting PAX8 directly holds greater therapeutic promise over targeting downstream effectors because these effectors vary depending on the cell of origin. Furthermore, we show through the use of micelle encapsulation that thiostrepton-SSM is an effective nanomedicine to target PAX8 in human HGSOC.

Supplementary Material

Refer to Web version on PubMed Central for supplementary material.

Acknowledgments

This work was supported by the Department of Defense Ovarian Cancer Fund 160076, the National Cancer Institute F30CA224986, the National Cancer Center for Research Resources Facilities Improvement Program C06RR15482, the University of Illinois-Chicago Department of Chemistry, the Ara Parsegian Medical Research Foundation, and the Abraham Lincoln Fellowship.

References

1. Siegel RL, Miller KD, Jemal A. Cancer statistics, 2017. CA Cancer J Clin 2017; 67: 7–30. [PubMed: 28055103]
2. Ozcan A, Shen SS, Hamilton C, Anjana K, Coffey D, Krishnan B et al. PAX 8 expression in non-neoplastic tissues, primary tumors, and metastatic tumors: a comprehensive immunohistochemical study. Mod Pathol 2011; 24: 751–764. [PubMed: 21317881]
3. McCloskey CW, Goldberg RL, Carter LE, Gamwell LF, Al-Hujaily EM, Collins O et al. A new spontaneously transformed syngeneic model of high-grade serous ovarian cancer with a tumor-initiating cell population. Front Oncol 2014; 4: 53. [PubMed: 24672774]
4. Tanwar PS, Mohapatra G, Chiang S, Engler DA, Zhang L, Kaneko-Tarui T et al. Loss of LKB1 and PTEN tumor suppressor genes in the ovarian surface epithelium induces papillary serous ovarian cancer. Carcinogenesis 2014; 35: 546–553. [PubMed: 24170201]
5. Rodgers LH, Ó hAinmhire E, Young AN, Burdette JE. Loss of PAX8 in high-grade serous ovarian cancer reduces cell survival despite unique modes of action in the fallopian tube and ovarian surface epithelium. Oncotarget 2016; 7: 32785–32795. [PubMed: 27129161]
6. Di Palma T, Lucci V, de Cristofaro T, Filippone MG, Zannini M. A role for PAX8 in the tumorigenic phenotype of ovarian cancer cells. BMC Cancer 2014; 14: 292. [PubMed: 24766781]
7. Piek JM, van Diest PJ, Zweemer RP, Jansen JW, Poort-Keesom RJ, Menko FH et al. Dysplastic changes in prophylactically removed Fallopian tubes of women predisposed to developing ovarian cancer. J Pathol 2001; 195: 451–456. [PubMed: 11745677]
8. Labidi-Galy SI, Papp E, Hallberg D, Niknafs N, Adleff V, Noe M et al. High grade serous ovarian carcinomas originate in the fallopian tube. Nat Commun 2017; 8: 1093. [PubMed: 29061967]
9. Kurman RJ, Shih I-M. Molecular pathogenesis and extraovarian origin of epithelial ovarian cancer--shifting the paradigm. Hum Pathol 2011; 42: 918–931. [PubMed: 21683865]
10. Elias KM, Emori MM, Westerling T, Long H, Budina-Kolomets A, Li F et al. Epigenetic remodeling regulates transcriptional changes between ovarian cancer and benign precursors. JCI Insight 2016; 1. doi:10.1172/jci.insight.87988.
11. Adler EK, Corona RI, Lee JM, Rodriguez-Malave N, Mhawech-Fauceglia P, Sowter H et al. The PAX8 cistrome in epithelial ovarian cancer. Oncotarget 2017; 8: 108316–108332. [PubMed: 29312534]
12. Mansouri A, Chowdhury K, Gruss P. Follicular cells of the thyroid gland require Pax8 gene function. Nat Genet 1998; 19: 87–90. [PubMed: 9590297]
13. Li CG, Nyman JE, Braithwaite AW, Eccles MR. PAX8 promotes tumor cell growth by transcriptionally regulating E2F1 and stabilizing RB protein. Oncogene 2011; 30: 4824–4834. [PubMed: 21602887]
14. Ghannam-Shahbari D, Jacob E, Kakun RR, Wasserman T, Korsensky L, Sternfeld O et al. PAX8 activates a p53-p21-dependent pro-proliferative effect in high grade serous ovarian carcinoma. Oncogene 2018; : 1–12.
15. Haley J, Tomar S, Pulliam N, Xiong S, Perkins SM, Karpf AR et al. Functional characterization of a panel of high-grade serous ovarian cancer cell lines as representative experimental models of the disease. Oncotarget 2016; 7: 32810–32820. [PubMed: 27147568]
16. King SM, Quartuccio SM, Vanderhyden BC, Burdette JE. Early transformative changes in normal ovarian surface epithelium induced by oxidative stress require akt upregulation, DNA damage, and epithelial-stromal interaction. Carcinogenesis 2013; : bgt003.

17. Eddie SL, Quartuccio SM, Ó hAinmhir E, Moyle-Heyrman G, Lantvit DD, Wei J-J et al. Tumorigenesis and peritoneal colonization from fallopian tube epithelium. Oncotarget 2015; 6: 20500–20512. [PubMed: 25971410]

18. Russo A, Czarnecki AA, Dean M, Modi DA, Lantvit DD, Hardy L et al. PTEN loss in the fallopian tube induces hyperplasia and ovarian tumor formation. Oncogene 2018; : 1.

19. Ran FA, Hsu PD, Wright J, Agarwala V, Scott DA, Zhang F. Genome engineering using the CRISPR-Cas9 system. Nat Protoc 2013; 8: 2281–2308. [PubMed: 24157548]

20. Endsley MP, Moyle-Heyrman G, Karthikeyan S, Lantvit DD, Davis DA, Wei J-J et al. Spontaneous Transformation of Murine Oviductal Epithelial Cells: A Model System to Investigate the Onset of Fallopian-Derived Tumors. Front Oncol 2015; 5: 154. [PubMed: 26236688]

21. Wiśniewski JR, Zougman A, Nagaraj N, Mann M. Universal sample preparation method for proteome analysis. Nat Methods 2009; 6: 359–362. [PubMed: 19377485]

22. Batth TS, Francavilla C, Olsen JV. Off-Line High-pH Reversed-Phase Fractionation for In-Depth Phosphoproteomics. J Proteome Res 2014; 13: 6176–6186. [PubMed: 25338131]

23. Gokce E, Andrews GL, Dean RA, Muddiman DC. Increasing proteome coverage with offline RP HPLC coupled to online RP nanoLC-MS. J Chromatogr B Analyt Technol Biomed Life Sci 2011; 879: 610–614.

24. Adusumilli R, Mallick P. Data Conversion with ProteoWizard msConvert. Methods Mol Biol Clifton NJ 2017; 1550: 339–368.

25. Ong S-E, Mann M. A practical recipe for stable isotope labeling by amino acids in cell culture (SILAC). Nat Protoc 2006; 1: 2650–2660. [PubMed: 17406521]

26. King SM, Hilliard TS, Wu LY, Jaffe RC, Fazleabas AT, Burdette JE. The impact of ovulation on fallopian tube epithelial cells: evaluating three hypotheses connecting ovulation and serous ovarian cancer. Endocr Relat Cancer 2011; 18: 627–642. [PubMed: 21813729]

27. Martiny-Baron G, Kazanietz MG, Mischak H, Blumberg PM, Kochs G, Hug H et al. Selective inhibition of protein kinase C isozymes by the indolocarbazole Gö 6976. J Biol Chem 1993; 268: 9194–9197. [PubMed: 8486620]

28. Ke N, Wang X, Xu X, Abassi YA. The xCELLigence system for real-time and label-free monitoring of cell viability In: Mammalian Cell Viability. Springer, 2011, pp 33–43.

29. Esparza K, Onyuksel H. Development of co-solvent freeze-drying method for the encapsulation of water-insoluble thiostrepton in sterically stabilized micelles. Int J Pharm 2019; 556: 21–29. [PubMed: 30529660]

30. de Cristofaro T, Di Palma T, Soriano AA, Monticelli A, Affinito O, Cocozza S et al. Candidate genes and pathways downstream of PAX8 involved in ovarian high-grade serous carcinoma. Oncotarget 2016; 7: 41929–41947. [PubMed: 27259239]

31. Hegde NS, Sanders DA, Rodriguez R, Balasubramanian S. The transcription factor FOXM1 is a cellular target of the natural product thiostrepton. Nat Chem 2011; 3: 725–731. [PubMed: 21860463]

32. Wang M, Gartel AL. Micelle-Encapsulated Thiostrepton as an Effective Nanomedicine for Inhibiting Tumor Growth and for Suppressing FOXM1 in Human Xenografts. Mol Cancer Ther 2011; 10: 2287–2297. [PubMed: 21903609]

33. Jiang L, Wu X, Wang P, Wen T, Yu C, Wei L et al. Targeting FoxM1 by thiostrepton inhibits growth and induces apoptosis of laryngeal squamous cell carcinoma. J Cancer Res Clin Oncol 2015; : 1–11.

34. Ashok B, Arleth L, Hjelm RP, Rubinstein I, Onyüksel H. In vitro characterization of PEGylated phospholipid micelles for improved drug solubilization: effects of PEG chain length and PC incorporation. J Pharm Sci 2004; 93: 2476–2487. [PubMed: 15349957]

35. Lim SB, Banerjee A, Önyüksel H. Improvement of drug safety by the use of lipid-based nanocarriers. J Control Release Off J Control Release Soc 2012; 163: 34–45.

36. Laury AR, Hornick JL, Perets R, Krane JF, Corson J, Drapkin R et al. PAX8 reliably distinguishes ovarian serous tumors from malignant mesothelioma. Am J Surg Pathol 2010; 34: 627–635. [PubMed: 20414098]

37. Cheung HW, Cowley GS, Weir BA, Boehm JS, Rusin S, Scott JA et al. Systematic investigation of genetic vulnerabilities across cancer cell lines reveals lineage-specific dependencies in ovarian cancer. Proc Natl Acad Sci U S A 2011; 108: 12372–12377. [PubMed: 21746896]

38. Musrap N, Tuccitto A, Karagiannis GS, Saraon P, Batruch I, Diamandis EP. Comparative Proteomics of Ovarian Cancer Aggregate Formation Reveals an Increased Expression of Calcium-activated Chloride Channel Regulator 1 (CLCA1). J Biol Chem 2015; 290: 17218–17227. [PubMed: 26004777]

39. Grassi ML, Palma C de S, Thomé CH, Lanfredi GP, Poersch A, Faça VM. Proteomic analysis of ovarian cancer cells during epithelial-mesenchymal transition (EMT) induced by epidermal growth factor (EGF) reveals mechanisms of cell cycle control. J Proteomics 2017; 151: 2–11. [PubMed: 27394697]

40. Waldemarson S, Krogh M, Alaiya A, Kirik U, Schedvins K, Auer G et al. Protein expression changes in ovarian cancer during the transition from benign to malignant. J Proteome Res 2012; 11: 2876–2889. [PubMed: 22471520]

41. Wang L-N, Tong S-W, Hu H-D, Ye F, Li S-L, Ren H et al. Quantitative proteome analysis of ovarian cancer tissues using a iTRAQ approach. J Cell Biochem 2012; 113: 3762–3772. [PubMed: 22807371]

42. Harms JM, Wilson DN, Schluenzen F, Connell SR, Stachelhaus T, Zaborowska Z et al. Translational regulation via L11: molecular switches on the ribosome turned on and off by thiostrepton and micrococcin. Mol Cell 2008; 30: 26–38. [PubMed: 18406324]

43. Cancer Genome Atlas Research Network. Integrated genomic analyses of ovarian carcinoma. Nature 2011; 474: 609–615. [PubMed: 21720365]

44. Zhang X, Cheng L, Minn K, Madan R, Godwin AK, Shridhar V et al. Targeting of mutant p53-induced FoxM1 with thiostrepton induces cytotoxicity and enhances carboplatin sensitivity in cancer cells. Oncotarget 2014; 5: 11365–11380. [PubMed: 25426548]

45. Cristofaro T de, Mascia A, Pappalardo A, D'Andrea B, Nitsch L, Zannini M. Pax8 protein stability is controlled by sumoylation. J Mol Endocrinol 2009; 42: 35–46. [PubMed: 18974227]

A

Proteomic analysis of OVCAR8 after PAX8 deletion

Gene ontology pathway	P value	Hits in pathway
Cytoskeleton structure	0.0005	11
Microtubule binding	0.001	15
Chaperone binding	0.001	9
Cytoskeletal protein binding	0.001	7
Ubiquitin protein ligase binding	0.007	16
Protein kinase binding	0.018	18
Cadherin binding involved in cell-cell adhesion	0.0038	14

B

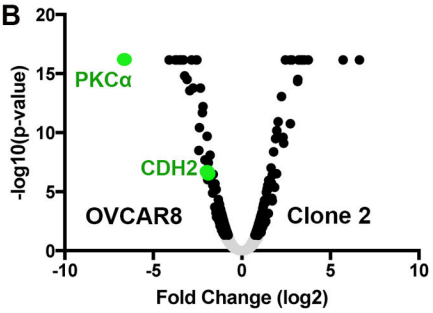

C

Proteomic analysis of MOSE after PAX8 overexpression

Gene ontology pathway	P value	Hits in pathway
Cadherin binding involved in cell-cell adhesion	3.5E-47	83
Oxidoreductase activity	1.4E-11	64
Ubiquitin protein ligase binding	8.6E-9	36
Actin binding	7.6E-8	67
Ran GTPase binding	5.5E-6	10
Integrin binding	2.5E-4	14
Cytoskeletal protein binding	4.7E-4	11

D

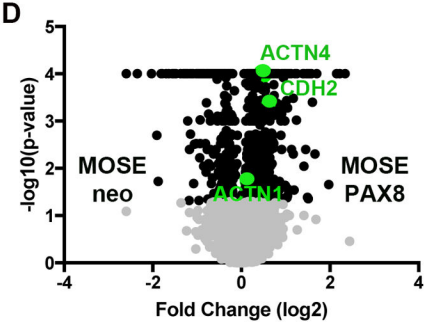

Figure 1. Proteomic analysis of PAX8 regulated pathways in OVCAR8^{RFP} and MOSE cells.

(A) Gene ontology (GO) analysis of PAX8 target proteins differentially expressed between OVCAR8^{RFP} and OVCAR8^{RFP}PAX8$^{-/-}$ clone 2. (B) Volcano plot of the pairwise comparison between OVCAR8^{RFP} and clone 2. Expression fold change (log 2) were plotted against the t-test p value (-log10). Proteins on the left side of the plot indicates their higher expression in OVCAR8^{RFP} cells. (C) GO analysis of PAX8 target genes differentially expressed between MOSE-neo and MOSE-PAX8 cells. (D) Volcano plot of the pairwise comparison between MOSE-neo and MOSE-PAX8 cells. Proteins on the right side of the plot indicates their higher expression in MOSE-PAX8 cells.

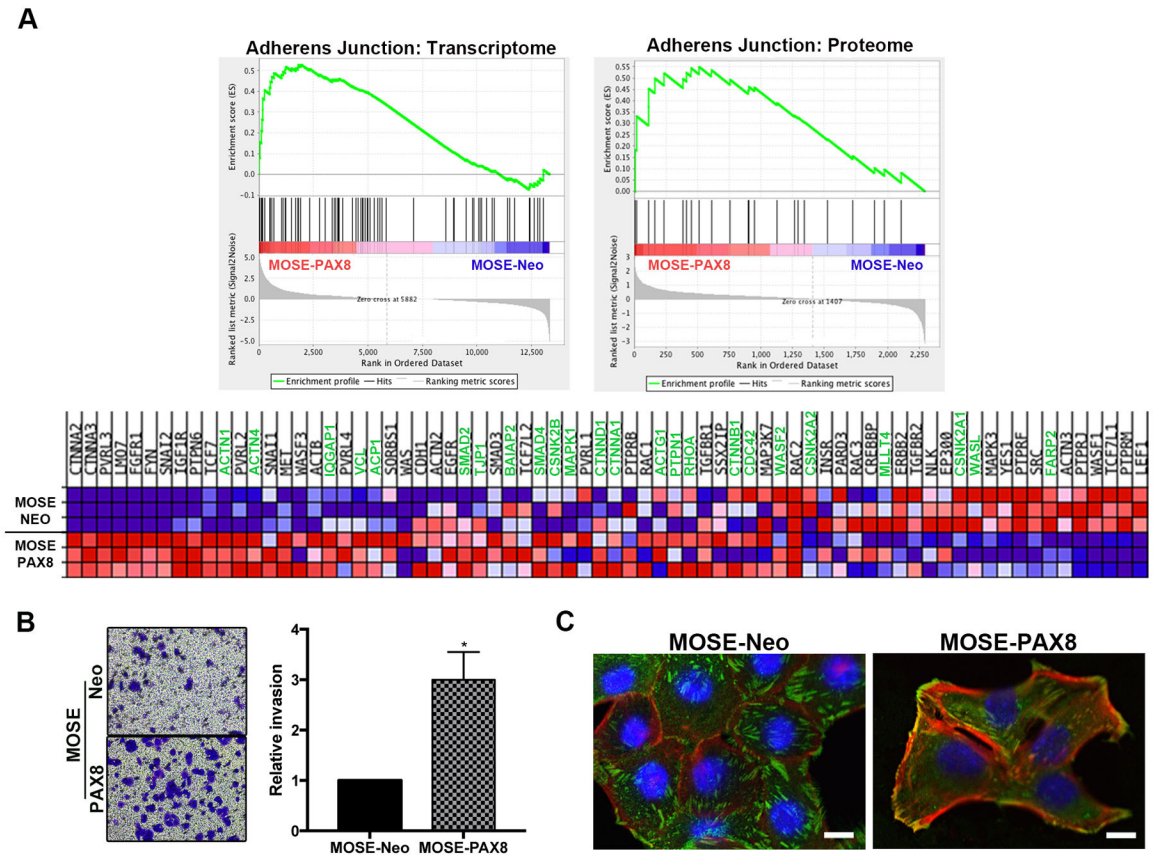

Figure 2. Transcriptome and proteome analysis identifies PAX8 regulates adherens junctions in the OSE.

(A) Gene set enrichment analysis (GSEA) of the transcriptome and proteome of MOSE-Neo and MOSE-PAX8 cells identified the adherens junction pathway as differentially regulated by PAX8. Gene names in the heat map labeled in green indicate genes that are drivers of adherens junctions in both the transcriptome and proteome of MOSE-PAX8 cells. (B) Relative invasion of MOSE-PAX8 cells over MOSE-Neo cells using a Boyden chamber assay. Cells that have invaded through matrigel are stained with crystal violet and quantified using microscopy (n=3, error bars = SEM). (C) Confocal imaging of MOSE-Neo and MOSE-PAX8 cells for actin (red), vinculin (green), and colocalization (yellow) of these proteins. Colocalization of actin and vinculin at the cell surface is a marker of adherens junctions. Scale bar, 10μM.

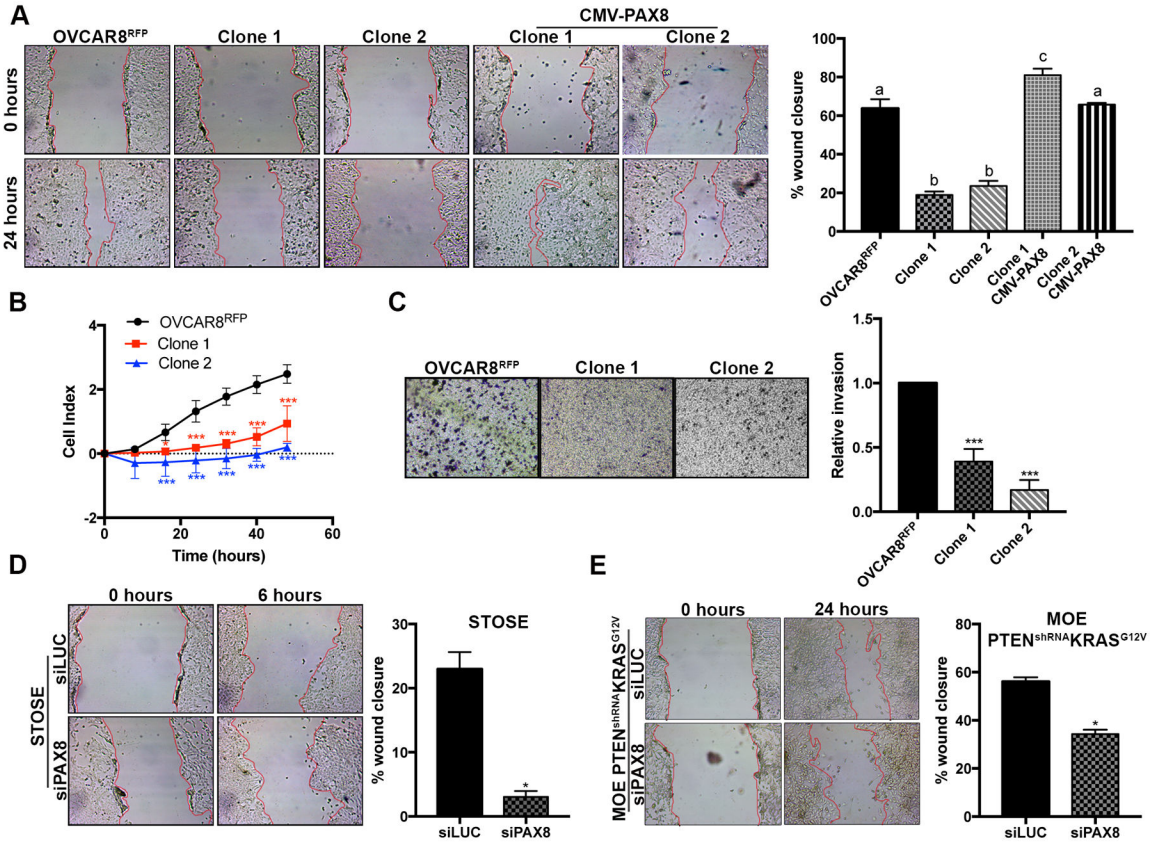

Figure 3. PAX8 deletion reduces the migratory potential of HGSOC, regardless of cell of origin.

(A) Wound closure assay over 24 hours to monitor migration in OVCAR8^{RFP}, OVCAR8^{RFP}PAX8$^{-/-}$ clone 1 and clone 2, and CMV-PAX8 transfected clone 1 and clone 2 cells. The percent wound closure for each cell line was quantified and represented in the bar graph. Means that do not share a letter are significantly different at $p<0.05$. (B) The xCELLigence real time cell analyzer was used to monitor migration over 48 hours. Cell index is a measure of electron impedance caused by migrating cells towards a serum chemoattractant. (C) Boyden chamber invasion assay through matrigel. Cell that have invaded are stained with crystal violet and quantified using microscopy. Relative invasion was determined as a ratio compared to OVCAR8^{RFP}. (D) Wound closure assay performed over 6 hours with the OSE derived tumor cell line STOSE transfected with RNAi for siLUC (control) or siPAX8 (experimental). (E) Wound closure assay performed over 24 hours with the oviductal derived tumor cell line MOE PTEN^{shRNA} KRAS^{G12V} cells transfected with RNAi for siLUC or siPAX8. Error bars for all assays represent standard errors for three replicates (n=3, error bars = SEM).

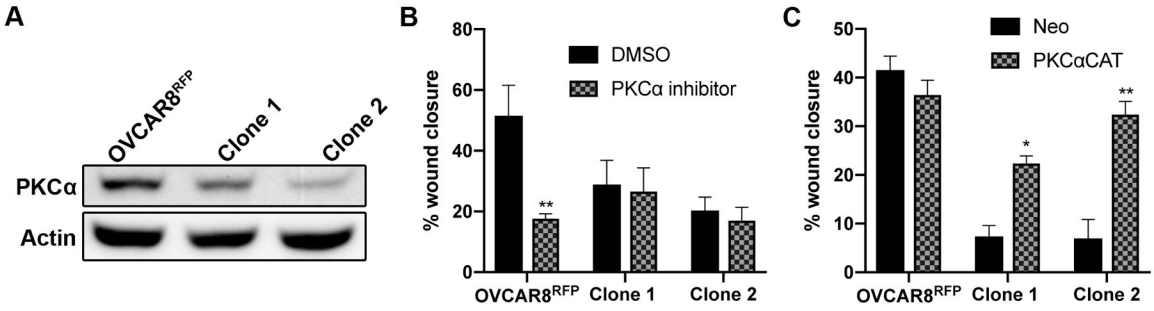

Figure 4. PAX8 upregulates PKCα in HGSOC to induce migration.

(A) Representative immunoblot of OVCAR8^{RFP} and OVCAR8^{RFP}PAX8$^{-/-}$ clone 1 and clone 2 demonstrates PAX8 deletion reduces PKCα levels. (B) Wound closure assay performed with OVCAR8^{RFP} and OVCAR8^{RFP}PAX8$^{-/-}$ clone 1 and clone 2 exposed to DMSO (control) or 5nM Go6976 (experimental) inhibitor against PKCα. (C) Wound closure assay performed over 24 hours with OVCAR8^{RFP} and OVCAR8^{RFP}PAX8$^{-/-}$ clone 1 and clone 2 transfected with neomycin vector (control) or PKCαCAT vector (experimental) containing the PKCα catalytic site. Error bars for all assays represent standard errors for three replicates (n=3, error bars = SEM).

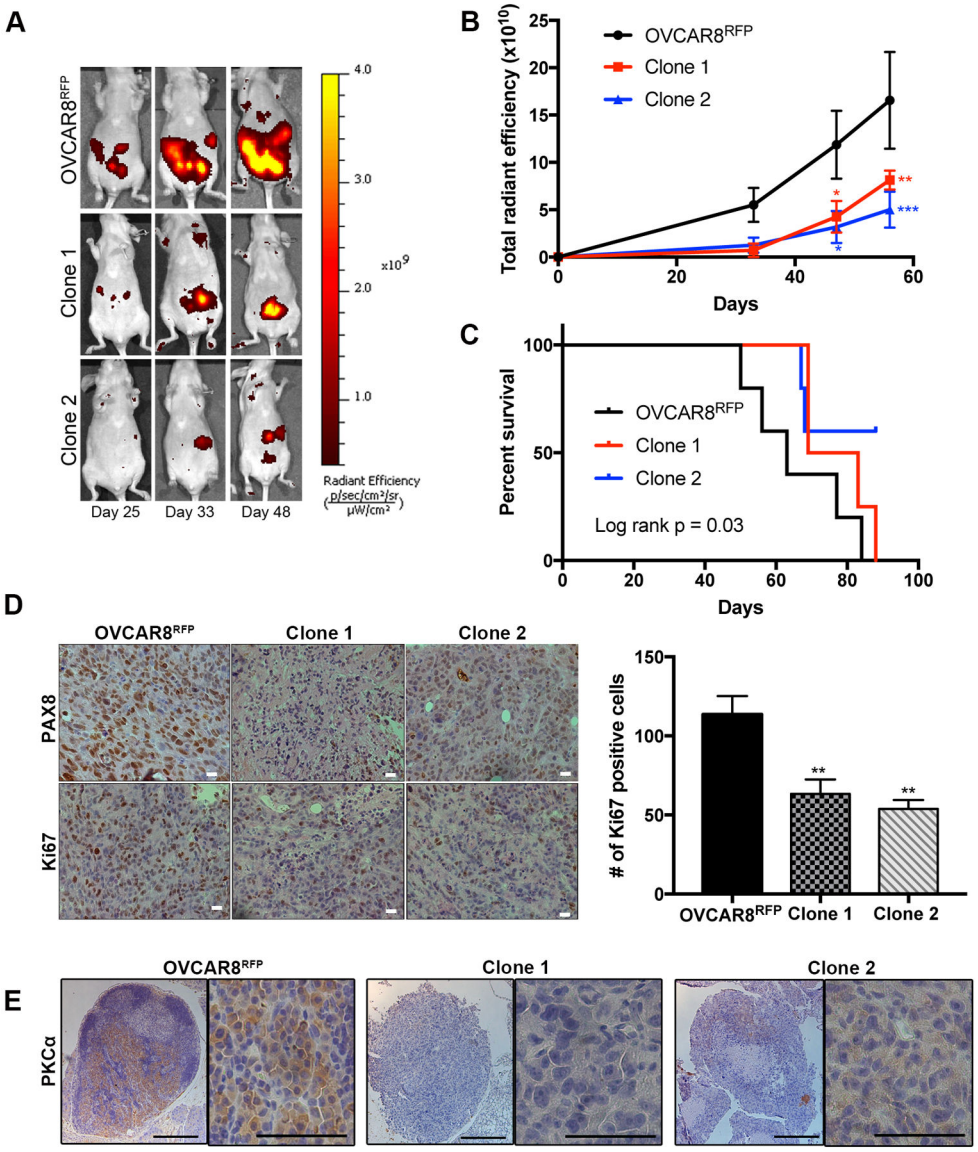

Figure 5. PAX8 deletion decreases tumor growth and increases survival in the HGSOC cell line OVCAR8^{RFP}.

(A) IVIS imaging of total radiant efficiency in athymic nude mice injected i.p. with OVCAR8^{RFP} and OVCAR8^{RFP}PAX8$^{-/-}$ clone 1 and clone 2. (B) Quantification of total radiant efficiency obtained using IVIS imaging demonstrates reduction in tumor burden after PAX8 deletion (n=5, error bars = SEM). (C) Kaplan-Meier percent survival curve analyzed by Logrank test (n=5, p=0.03). (D) IHC using PAX8 antibody indicates stable PAX8 deletion *in vivo* for OVCAR8^{RFP}PAX8$^{-/-}$ clone 1 and clone 2. IHC using Ki67 antibody indicates decreased proliferation in clone 1 and clone 2. Scale bar, 10μM. Quantification of Ki67 was performed using four representative images (n=4, error bars = SEM). (E) IHC using PKCα specific antibody verifies that PAX8 deletion reduces PKCα levels *in vivo*. Scale bar, 100μM.

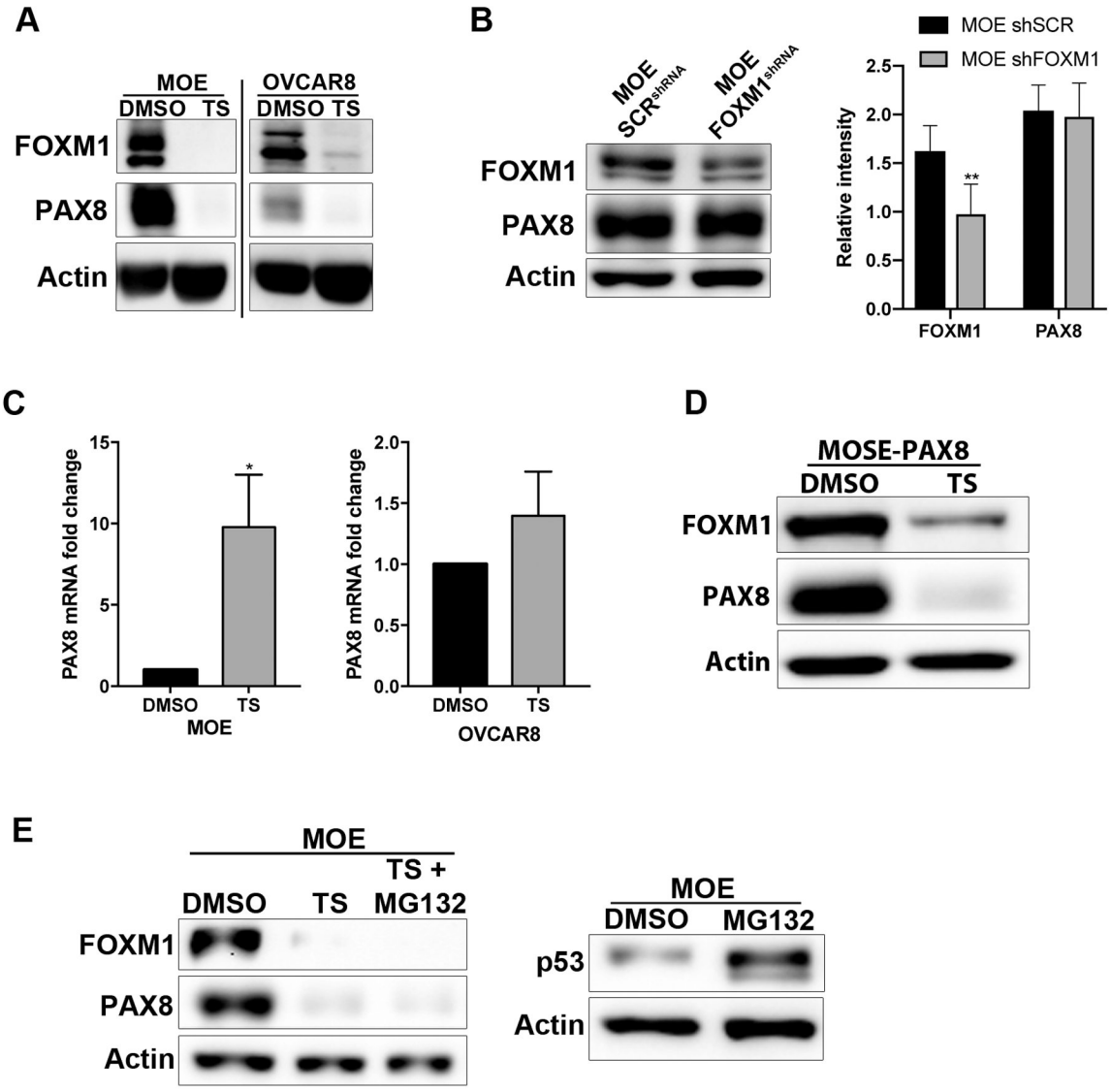

Figure 6. Thiostrepton destabilizes PAX8 protein through a proteasome independent pathway.

(A) Immunoblot in MOE and OVCAR8 cells exposed to 10uM thiostrepton (TS) demonstrates a reduction in FOXM1 and PAX8 protein. (B) Immunoblot demonstrating FOXM1 knockdown does not affect PAX8 protein levels in MOE cells. Densitometry was performed to quantify the protein levels of FOXM1 and PAX8. (C) RT-PCR for PAX8 after exposure to thiostrepton. Fold change was determined compared to DMSO control (n=3, error bars = SEM). (D) Immunoblot demonstrating reduction in PAX8 and FOXM1 in MOSE cells exposed to thiostrepton even after transfection with constitutively active CMV-PAX8 promoter (MOSE-PAX8). (E) Immunoblot for PAX8 and FOXM1 in MOE cells exposed to thiostrepton (10μM) or combination treatment with proteasome inhibitor MG132 (10μM). MG132 stabilizes p53, a positive control for proteasome inhibition.

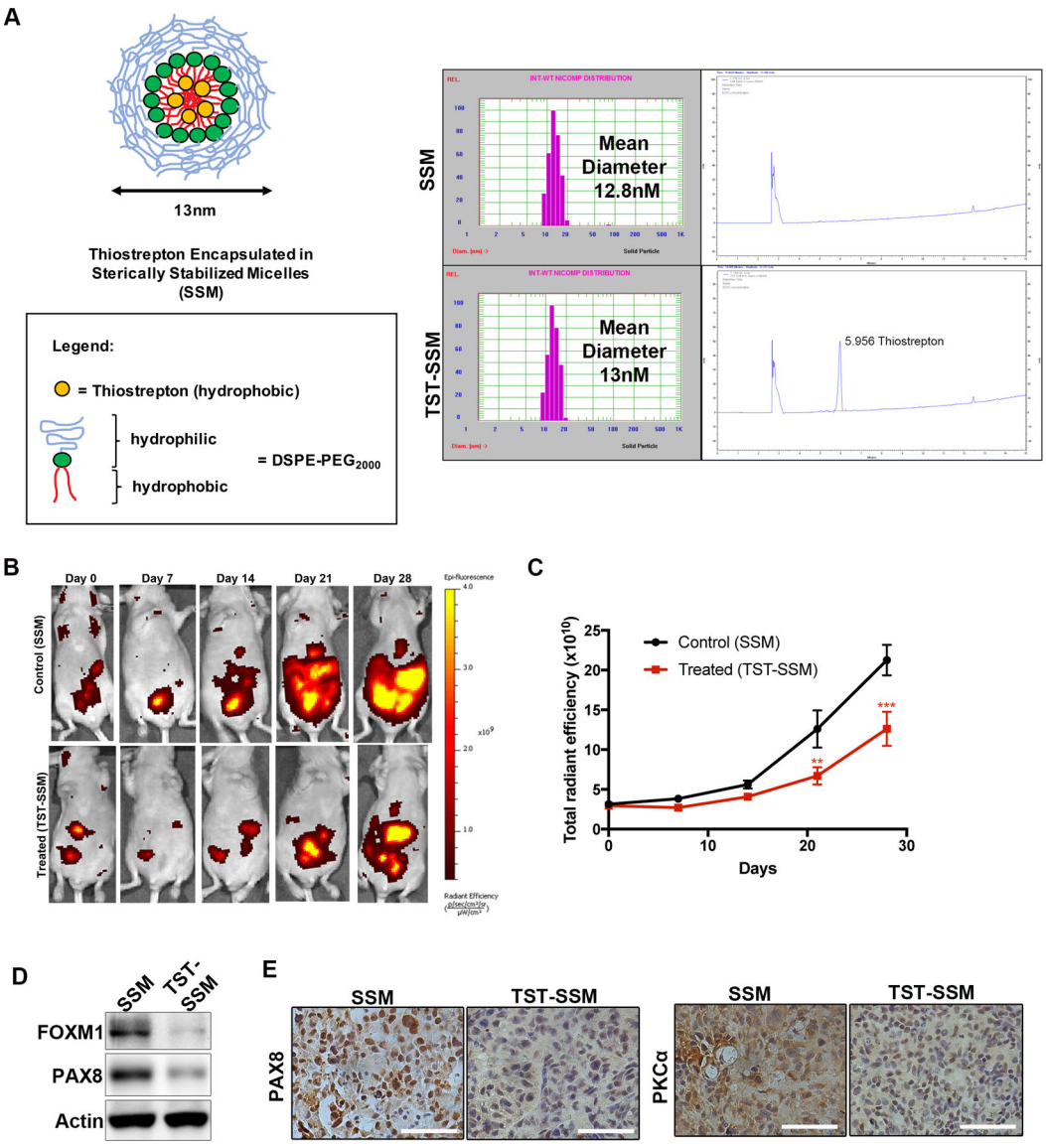

Figure 7. Nanoparticle encapsulation of thiostrepton inhibits tumor growth of HGSOC.

(A) Schematic encapsulation of the hydrophobic thiostrepton drug in sterically stabilized micelles (SSM) composed of distearoylphosphatidylethanolamine (DSPE-PEG) with a PEG chain of 2000. Micelle particle size was analyzed by dynamic light scattering and the mean particle size was obtained from the Stokes-Einstein relation. Thiostrepton incorporation into the TST-SSM particle was determined by HPLC. (B) IVIS imaging of total radiant efficiency of OVCAR8^{RFP} injected i.p. in athymic nude mice. Mice were treated 3x per week with SSM (control) of TST-SSM (experimental) for 4 weeks (n=5, error bars = SEM). (C) Quantification of the total radiant efficiency obtained by IVIS imaging demonstrates reduced tumor burden in TST-SSM treated mice. (D) Immunoblot of tumor cells treated with SSM or TST-SSM demonstrates reduction in FOXM1 and PAX8 *in vivo*. (E) IHC demonstrates reduction in PAX8 and PKCα in tumors treated with TST-SSM.